Alternating Current Instability of Conduction-Cooled High-T_c Superconductors and Superconducting Tapes

V. R. Romanovskii[1*], K. Watanabe[2], A. M. Arkharov[3], S. Awaji[2], N. A. Lavrov[3] and V. K. Ozhogina[1]

[1]*NBIKS-Center, National Research Center "Kurchatov Institute", Moscow 123182, Russia*
[2]*High Field Laboratory for Superconducting Materials, Institute for Materials Research, Tohoku University, Sendai 980-8577, Japan.*
[3]*Moscow State Bauman Technical University, Moscow 107005, Russia.*

Authors' contributions

This work was carried out in collaboration between all authors. All authors read and approved the final manuscript.

ABSTRACT

The AC current instability mechanisms are investigated in high-T_c superconductor and superconducting tape at conduction-cooled conditions when the electric field and applied current may essentially exceed the critical values of a superconductor. It is shown that there exist the characteristic times defining the corresponding time windows that are the basis of the existence of the stable AC regimes despite the high values of the induced electric field and the temperature of a superconductor. It is proved that these values are higher than the corresponding values of the electric field and the temperature before the thermal runaway. These states may be defined as stable overloaded regimes. Therefore, high-T_c superconducting magnets are possible to operate stably at AC overloaded regimes and the conduction-cooled conditions, which will be characterized by very high AC losses.

Corresponding author: Email: vromanovskii@netscape.net;

1. INTRODUCTION

The macroscopic electrodynamics investigations of superconductors are one of the most fundamental issues for both low-T_c and high-T_c superconductors. It is important for the understanding of the superconductivity mechanisms [1-3]. Therefore, the increasing use of superconductors for advanced applications has generated much interest in such study.

The study of current-carrying capacity of superconductors is one of main problems of applied superconductivity [4,5]. The limiting currents flowing stably in low-T_c superconductors, which have steep voltage-current characteristics, are often defined by a priory chosen value of the critical electric field used in the definition of the critical current during DC measurements [4,5]. However, high-T_c superconductors have a broad shape of the voltage-current characteristics. Therefore, the finite voltage is induced long before the current instability onset in high-T_c superconductors. In these states, superconductors are in resistive modes even in the low electric field range [6]. Nevertheless, the voltage-current characteristics are widely used to determine the critical current of high-T_c superconductors as their basic property. At the same time, a lot of experimental and theoretical investigations (see, for example, [7-9]) prove that resistive states of high-T_c superconductors can be stable at higher electric fields and currents than the critical ones following from the fixed electric field criterion. These features lead to the thermal runaway concept, which must be used to find the stability boundary of charging current.

In the macroscopic approximation, the formulation of the current stability conditions must be based on the analysis of violation of thermal equilibrium of superconductor's electrodynamics states, as it was formulated for the first time in [10] for fully penetrated current states of low-T_c superconductors. Using this idea, the current-carrying capacities of high-T_c superconductors and superconducting tapes have been investigated in detail during DC operating modes (see, for example, [7-9,11-20] and references cited therein). However, the basic thermal and electrodynamics formation features of stable and unstable AC regimes of the high-T_c superconductors have still not been discussed.

In the investigation presented below, we extend the thermal runaway concept on the AC operating modes. It allows us to formulate the basic thermal and electrodynamics features of the current instability onset in high-T_c superconductors during alternating current charging.

2. THERMO-ELECTRODYNAMICS MODELS

The theoretical analysis of the macroscopic AC phenomena in superconducting current-carrying elements must be based on the numerical solution of the multidimensional equations that allows one to describe the evolution of their thermal and electrodynamics states. However, such modeling is cumbersome and time-consuming because of the complexity of computation models, which, as a rule, are based on the use of the finite element method (see, for example, [14,21,22]). Simpler models are preferable to understand the stability mechanisms of AC regimes under which superconducting power devices are operated.

Let us consider a superconductor with a slab geometry (-a<x<a, -b<y<b, -∞<z<∞, b>>a) placed in a constant external magnetic field parallel to its surface in the *y*-direction that is penetrated over its cross section (S=4ab). Suppose that the applied current is charged in the *z*-direction increasing in time as sine function (I=$I_m$sin2πft) with frequency *f* and its self-

magnetic field is negligibly lower than the external magnetic field. Let us describe the voltage-current characteristic of the superconductor by a power law and approximate the dependence of the critical current on the temperature by the linear relationship [4,5]. Assume also that the superconductor has the transverse size in the *x*-direction, which does not lead to the magnetic instability. Therefore, the transient one-dimensional equations describing the evolution of the temperature $T(x,t)$ and the electric field $E(x,t)$ inside the superconducting slab is independent of *z* and *y* coordinates and may be written as follows

$$C(T)\frac{\partial T}{\partial t} = \frac{\partial}{\partial x}\left(\lambda(T)\frac{\partial T}{\partial x}\right) + EJ \tag{1}$$

$$\mu_0 \frac{\partial J}{\partial t} = \frac{\partial^2 E}{\partial x^2}, \quad t > 0, \quad 0 < x < a \tag{2}$$

Here, the electric field, the current density $J(x,t)$ and the critical current density $J_c(T,B)$ conform the following relationships

$$E = E_c \left[J / J_c(T,B)\right]^n \tag{3}$$

$$J_c(T) = J_{c0}\left(T_{cB} - T\right)/\left(T_{cB} - T_0\right) \tag{4}$$

For the problem under consideration, the initial and boundary thermo-electrodynamics conditions are given by

$$T(x,0) = T_0, \quad E(x,0) = 0, \tag{5}$$

$$\frac{\partial T}{\partial x}(0,t) = 0, \quad \lambda\frac{\partial T}{\partial x}(a,t) + h\left[T(a,t) - T_0\right] = 0, \tag{6}$$

$$\frac{\partial E}{\partial x}(0,t) = 0, \quad \frac{\partial E}{\partial x}(a,t) = \frac{\mu_0}{4b}\frac{dI}{dt} \tag{7}$$

Here, *C* and λ are the specific heat capacity and thermal conductivity of the superconductor, respectively; *h* is the heat transfer coefficient; T_0 is the cooling bath temperature; *n* is the power law exponent of the *E-J* relation; E_c is the voltage criterion defining the critical current density of the superconductor; J_{c0} and T_{cB} are the known constants at the given external magnetic field *B*.

The model defined by equations (1) – (7) may be simplified in the cases when the temperature, electric field and current distributions inside the superconductor are practically uniform. Integrating equation (1) with respect to *x* from 0 to *a* and considering the boundary conditions (6), it is easy to get the following transient heat balance equation

$$C(T)\frac{dT}{dt} = -\frac{h}{a}(T - T_0) + E(t)J(t) \tag{8}$$

This equation with the relations (3) and (4) describes the uniform time variation of the temperature and the electric field as a function of charged current $I(t)=J(t)S$.

As it is well known, the critical properties of Bi-based superconductors essentially exceed critical properties of low-T_c superconductors in high magnetic fields. This opens up many kinds of applications of these superconductors. For example, a conduction-cooled Bi2212-magnet is one of possible new generations of a high field magnet system [23-29]. In this connection, let us investigate the physical features of stable and unstable AC formation of thermo-electrodynamics states in the current charging into a Bi2212-superconductor under non-intensive cooling conditions, which take place in conduction-cooled magnets [25].

Fig. 1 shows zero-dimensional and one-dimensional simulation results of the initial stages of the stable waveform evolution of the electric field and the temperature in the slab. The insets show the corresponding curves in more detail. The simulation was made for a initially cooled $Bi_2Sr_2CaCu_2O_8$ slab (a = 10^{-3} cm, b = 10^{-2} cm) at T_0=4.2 K, h=10^{-3}W/ ($cm^2 \times$K) and B=10 T. The results presented were based on the numerical solution of the problem defined by equations (1) - (8) at I_m=0.935 A, f = 10 Hz. The specific heat capacity and thermal conductivity of the superconductor were defined as follows

$$C\left[\frac{J}{cm^3 \cdot K}\right] = 10^{-6} \times \begin{cases} 58.5T + 22T^3, \ T \leq 10K \\ -10.54 \times 10^4 + 1.28 \times 10^4 T, \ T > 10K \end{cases}$$

$$\lambda(T)\left[\frac{W}{cm \cdot K}\right] =$$
$$(-1.234 \times 10^{-5} + 1.654 \times 10^{-4}T + 4.608 \times 10^{-6}T^2 - 1.127 \times 10^{-7}T^3 + 6.061 \times 10^{-10}T^4)$$

According to [30,31], respectively. The parameters of the superconductor were set as E_c = 10^{-6} V/cm, J_{c0} = 1.52×10^4 A/cm^2, T_{cB} = 26.12 K and n = 10 according to [32].

It is seen that the temperature evolution during the entire current charging mode is practically uniform in the cooling mode under consideration. Therefore, the electric field distribution is also practically uniform in the fully penetrated states. Accordingly, these simulations can be a reason, which permits to use zero-dimensional approximation. Moreover, to verify the formation features of AC thermo-electrodynamics states formulated below in the framework of the zero-dimensional model, the one-dimensional simulation of serrated current charging mode is presented in Appendix. By that, the below-discussed results were carried out under zero-dimensional model described by equations (3), (4) and (8) without a large amount of computing.
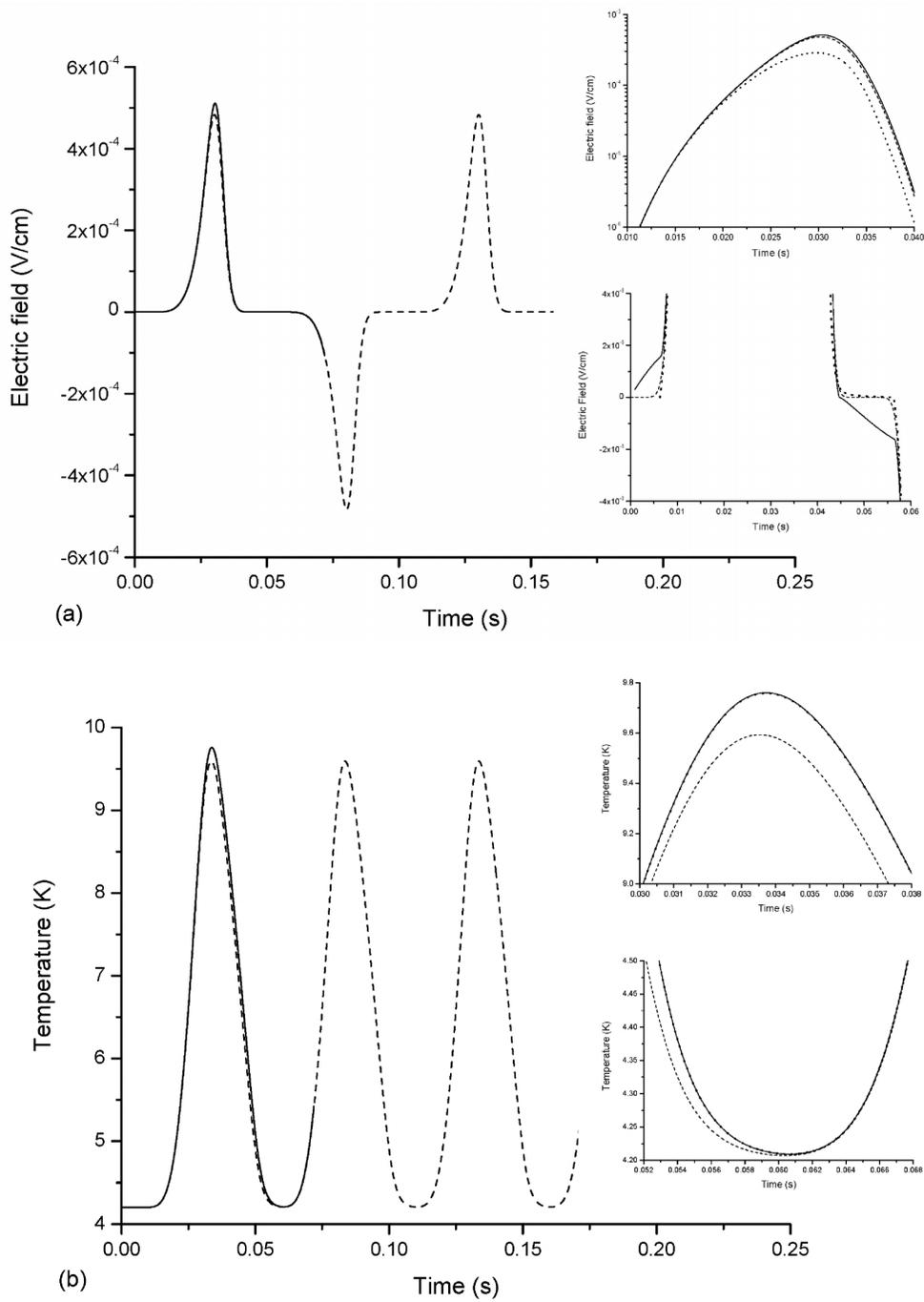
Fig. 1. Zero-dimensional (0D) and one-dimensional (1D) simulation of electric field (a) and temperature (b) induced in the AC regime: *- - - - 0D, ——— - 1D, x=a, …… - 1D, x=0*

3. AC STABILITY MECHANISMS OF SUPERCONDUCTING STATES

Fig. 2 shows the variation in time of the electric field, the temperature, the heat generation ($G = E(t)J(t)$) and the heat removal power ($W = h(T-T_0)/a$) in the considering superconducting slab at f = 10 Hz and different values of the peak current leading to the stable or unstable regimes. The corresponding curves calculated at f = 100 Hz are presented in Fig. 3. In these cases, the critical current of the superconductor and the thermal runaway current are equal to I_c = 0.61 A and I_q = 0.87 A, respectively. The corresponding thermal runaway values of the electric field and the temperature are equal to $E_q = 9 \times 10^{-5}$ V/cm and T_q = 6.16 K. They follow from the results presented in [33].

It is seen that stable and unstable AC regimes may exist in both input and output current charging modes. For example, the curves 3-5 in Figs. 2a and 2b correspond to the stable dynamics of the electric field and the temperature. They depict that the peak currents exceed not only the critical current but also the thermal runaway current. Therefore, the maximum stable values of electric field $|E_{max}|$ and temperature T_{max} are very high during these AC loads. Moreover, the corresponding peak values of the electric field and temperature are larger than the conformable thermal runaway values. This feature is due to very high stable heat power generated in the superconductor. Indeed, the peak value of the heat generation exceeds 20 W/cm^3 during operating mode under consideration. It exceeds the cooling power practically over 3 times. However, the superconducting properties of the slab are not destroyed in these intensive AC regimes despite such a significant difference. They may be defined as the overloaded regimes.

Figs. 2 and 3 depict that formation of stable and unstable cycles depends on the peak current and frequency. Besides, the frequency of the current load influences on the transition time after which peak values of electric field (and, thus, temperature) become practically constant during the stable AC overloaded regime. At the same time, an increase in the frequency may lead to the stabilization of the operational states. It is seen that the limiting peak values of the electric field and temperature at f = 10 Hz are higher than ones at f = 100 Hz during stable states. Therefore, the corresponding value of the peak current at f = 100 Hz exceeds one at f = 10 Hz.

Figs. 2 and 3 also prove that AC dynamics of the temperature or electric field has the similar nature that is observed near stability boundary at DC charging modes when the superconducting state may be either kept or lost [19,20]. Note that the bifurcation nature of DC charging modes near stability boundary has been established for the first time in [34] studying the ramp-rate limitation problem for low-T_c superconducting composites. The conclusions formulated in [34] have been permitted to understand the energy nature of the superconducting state stability problem. This feature that also takes place for high-T_c superconductors and superconducting tapes will be discussed below.

Thus, the limiting peak current must exist during AC regime. Therefore, if operating peak currents are below the limiting peak current then a superconductor saves its superconducting state. Otherwise the superconducting state is destroyed. This idea permits one to find the stability boundary of the AC regimes in the experiments during which two characteristic peak values will be determined. By that, the minimum peak value of charging current will correspond to the upper stable value of the peak current charged into the superconductor despite its high stable overheating. Accordingly, the maximum value of them will define the peak current at which the AC regimes are unstable.
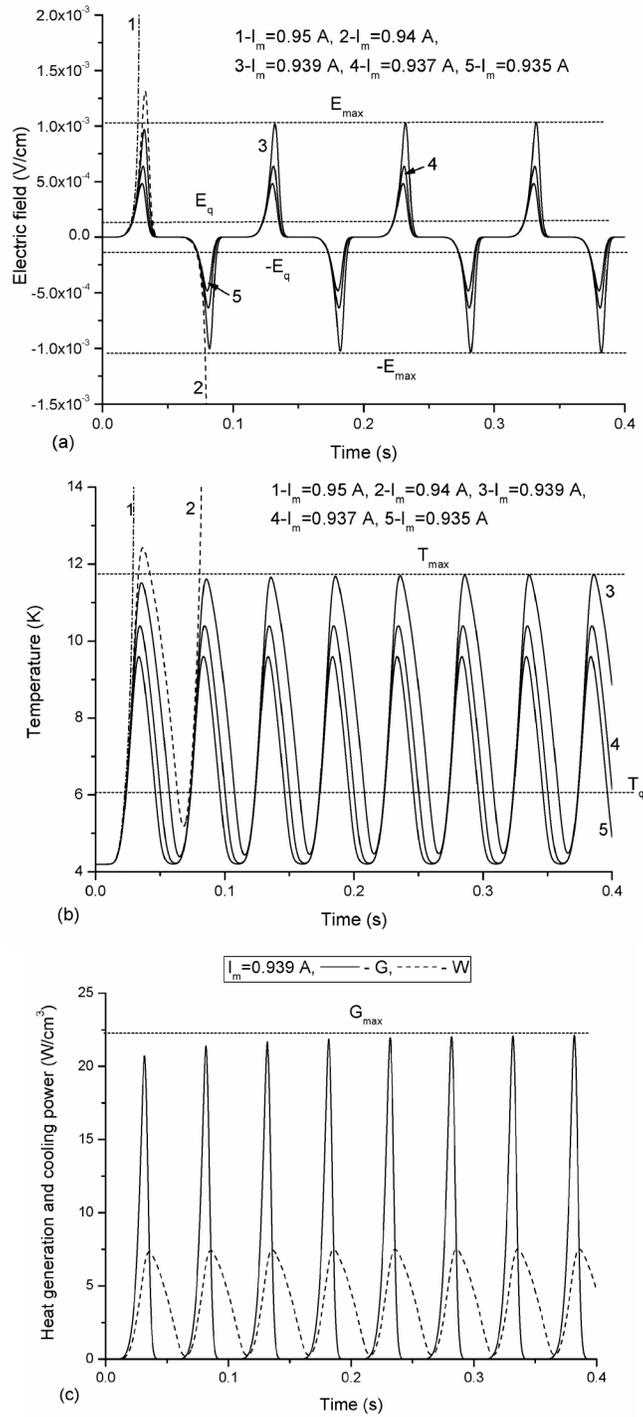
Fig. 2. Stable and unstable evolution of electric field (a), temperature (b), heat generation and cooling power (c) at *f* = 10 Hz
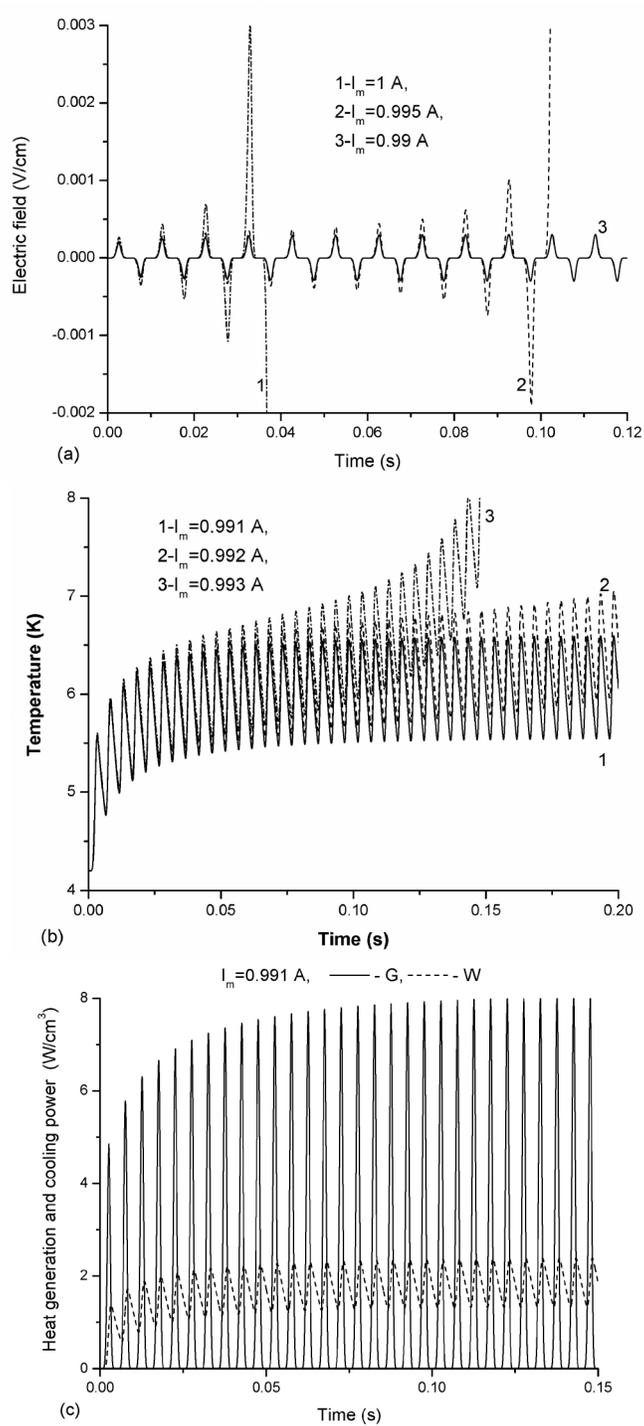
Fig. 3. Stable and unstable evolution of electric field (a), temperature (b), heat generation and cooling power (c) at *f* = 100 Hz

Let us discuss the mechanisms underlying the stable formation of AC overloaded regimes. Figs. 4 and 5 present the modeling results of the current charging when frequency has low or high values. They demonstrate the existence of the characteristic stable stages. The dynamics of the current, electric field and temperature is shown in Fig. 4a that take place after some transition time at f = 10 Hz and I_m = 0.939 A. The corresponding curves depict the heat removal and the heat generation in Fig. 4b. Fig. 5 illustrates the calculation results made at f = 100 Hz and I_m = 0.991 A. These figures allow one to explain the existence of stable AC overloaded regimes showing the presence of characteristic formation stages.
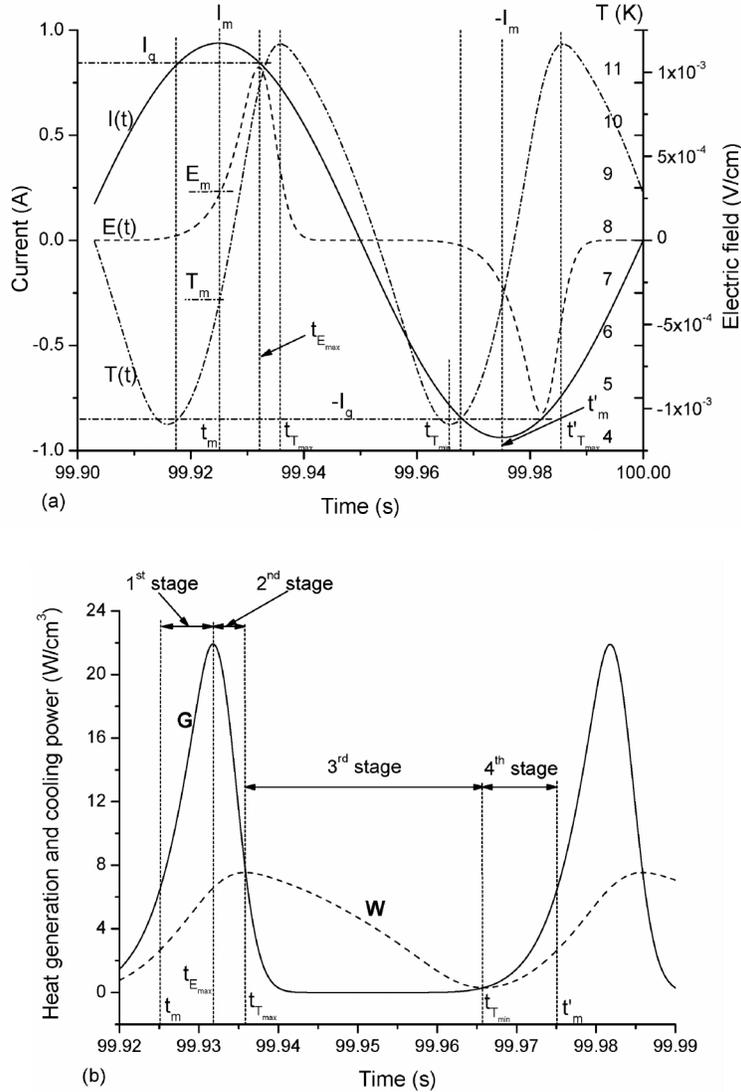

Fig. 4. Stable stages of AC overloaded regime at I_m= 0.939 A and f = 10 Hz:
a – charged current, temperature and electric field induced in superconductor, b – heat generation and cooling power

First of all, let us discuss the operational states that take place in the current charging with low frequency. In this case, the first stage starts at $t = t_m$ when the charged current equals peak value I_m. This stage exists in the interval $t_m < t < t_{Emax}$. Here, t_{Emax} is the time when the induced electric field has maximum (Fig. 4a). In this stage, the electric field and the temperature still increase from the corresponding values E_m and T_m despite the fact that the charged current decreases. Accordingly, increasing in the time the heat generation in a superconductor (G) exceeds the heat removal (W). At the same time, the heat generation has maximum at $t = t_{Emax}$ (Fig. 4b) after which the charged current becomes less than the corresponding value of the thermal runaway current I_q and an induced electric field begins to decrease.
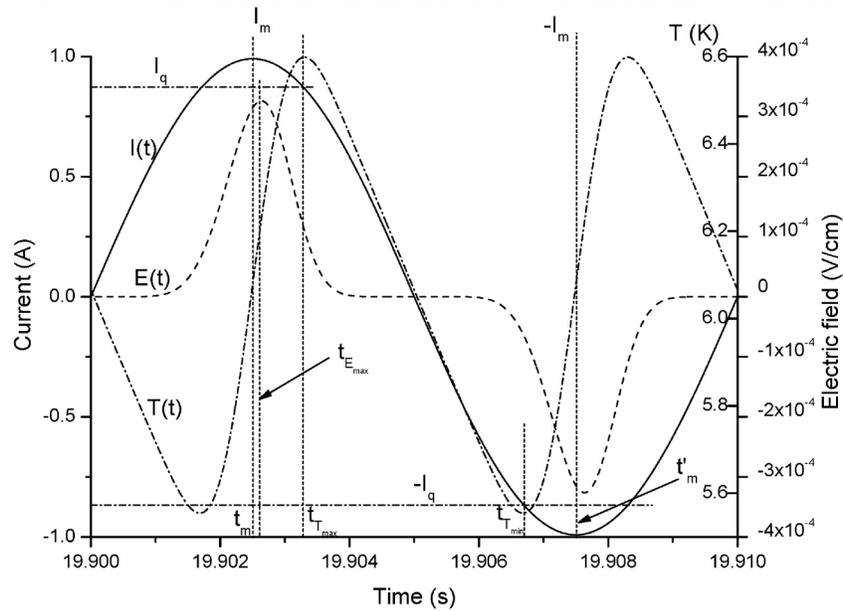

Fig. 5. Formation time windows of charged current, temperature and electric field at I_m= 0.991 A and f = 100 Hz

Note that the charged current is unstable in this stage as the charged current is still higher than the thermal runaway current. However, the instability does not occur because, first, the charged current decreases. Second, the electrodynamics state dynamics of superconductor depends essentially on the temperature dependence of the specific heat capacity when $E >$ E_c, as it was proved in [19,20] for DC regimes. Consequently, the rise of the electric field and the temperature becomes more stable both before and after instability onset. The role of $C(T)$ will be discussed below.

In the second stage that begins at $t > t_{Emax}$ the induced electric field start to decrease. This stage takes place due to the fact that the charged current not only decreases in time but becomes less than the thermal runaway current ($I(t) < I_q$). At the same time, the heat generation, which decreases, still is larger than the increasing in time the heat removal in the interval $t_{Emax} < t < t_{Tmax}$, as figure 4b depicts. Here, t_{Tmax} is the time where the heat generation equals the heat removal and then the temperature of a superconductor has maximum. That is why the temperature of the superconductor continues to rise in the second stage (Fig. 4a).

The mutual decrease of the charged current and the induced electric field leads to the stage when the heat generation becomes less than the heat flux to the coolant. It is the third stage beginning at $t > t_{\text{Tmax}}$, which is characterized by the stable decrease of the charged current, the electric field and the temperature (Fig. 4a). This stage ends at t_{Tmin}, which is the time when $G=W$. By that, the heat generation begins to exceed the heat removal in the interval $t > t_{\text{Tmin}}$. It is the fourth stage when the temperature of a superconductor again rises. At the end of this stage, the temperature of superconductor is equal to the conformable value T_{m} when the electric field and the current are equal to the corresponding peak values $-E_{\text{m}}$ and $-I_{\text{m}}$, respectively. Other AC stages repeat above-discussed ones and the stable evolution of the AC overloaded regime goes on.

Fig. 5 demonstrates the effect of high frequency on the formation of the AC stages. It is seen that the duration of the first stage ($t_{\text{m}} < t < t_{\text{Emax}}$) may essentially decrease. It becomes very short in comparison with the first stage that takes place at the low frequency. To be exact, the electric field practically starts to decrease when the charged current begins to decrease after t_{m}. Note that there exist operating regimes when the first stage may be absent. It is due to the fact that the frequency is high and the time, during which the instability develops, is short. The next stage exists at $t > t_{\text{Emax}}$. The electric field and, thus, the heat generation begin to decrease in this stage. However, the temperature of superconductor increases because the charged current is still in the unstable range ($I(t) > I_{\text{q}}$). The decreasing in time the heat generation leads to a time when the heat generation is equal to the cooling power. Therefore, the finish time boundary of the second stage is defined by t_{Tmax}, as discussed above for the low frequency current charging. At the same time, the value t_{Tmax} is also defined by the condition $I(t) = I_{\text{q}}$, as it follows from figure 5. It is the result of peculiarity according to which the charged current must be stable in the third stage ($t_{\text{Tmax}} < t < t_{\text{Tmin}}$) and the temperature will decrease at $I(t) < I_{\text{q}}$. The condition $I(t) = I_{\text{q}}$ also defines the t_{Tmin}, after which the charged current is not in the stable range, as it depicts Fig. 5. (Note that the value t_{Tmin} also follows from the balance condition between heat generation and cooling power.) Consequently, the temperature of superconductor starts to increase in the fourth stage ($t > t_{\text{Tmin}}$) because the charged current is higher than the thermal runaway current.

The obtained results show that the time windows of formation stages will depend on the frequency. As a result, the limiting current-carrying capacity of high-T_{c} superconductors also will depend on the frequency. As it will be shown below, it monotonically increases with increasing frequency. Besides, the discussed peculiarities influence on the shapes of the voltage-current characteristic during AC regimes. To illustrate this conclusion, the voltage-current characteristics during AC regimes are presented in Fig. 6 for two investigated modes. It is seen that they have hysteresis. It depends on the frequency. As a result, this feature leads to the fact that difference between the currents, at which the peak values of the current and the electric field exist, depends also on the frequency. Note that there exists the transition time when the voltage-current characteristics depend on the cycle duration. It should be taken into account in experiments.

Above discussed features may be justified on the basis of equations (1) and (2). They lead to the following relationship

$$\frac{dE}{dt} = \left\{ \frac{dI}{dt} + \frac{[G(T) - W(T)]S}{C(T)} \left| \frac{dJ_c}{dT} \right| \left(\frac{E}{E_c} \right)^{1/n} \right\} \frac{nE}{J_c(T)S} \left(\frac{E_c}{E} \right)^{1/n} \tag{9}$$
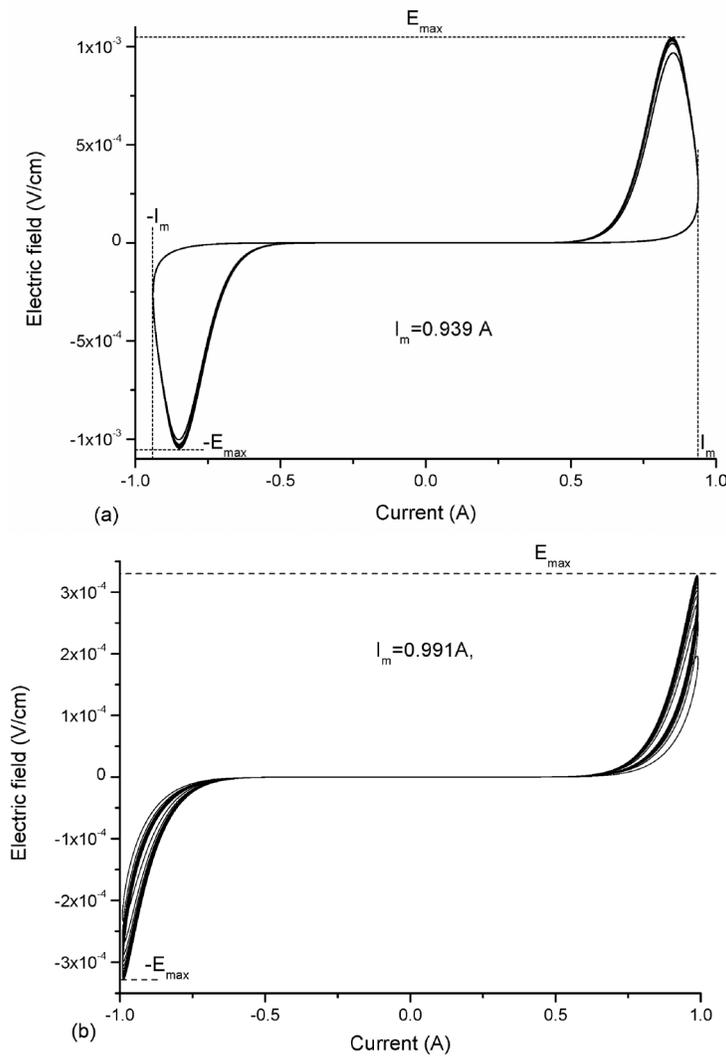
Fig. 6. Voltage-current characteristics of superconductor during stable AC overloaded regimes
(a) - f = 10 Hz, (b) - f = 100 Hz

that takes place in the current range when $E > 0$. It shows how difference between the maximum values of the current and the electric field depends on the mutual dynamics of charged current, induced electric field and temperature, in particular, frequency or the temperature dependences of the critical current of superconductor and its heat capacity. Indeed, the first discussed stage occurs when $dI/dt < 0$ and $G > W$. As follows from Figs. 2 and 3, the lower frequency, the higher difference between G and W and the higher induced electric field. Therefore, according to the equality (9), the higher frequency, the lower duration of the first stage. Moreover, the lower frequency, the higher temperature rise of superconductor, and then the higher influence of heat capacity. As a whole, when the condition

$$\left\|\frac{dI}{dt}\right\|_{t=t_{Emax}} \gg \left.\frac{(G-W)S}{C}\left|\frac{dJ_c}{dT}\right|\left(\frac{E}{E_c}\right)^{1/n}\right|_{t=t_{Emax}}$$

takes place then difference between t_m and t_{Emax} will be practically absent. Thus, the limiting peak current will weakly depend on the frequency when the latter will exceed the characteristic value.

The stability of the AC overloaded regimes may be explained considering the fluctuation of the corresponding average values of the temperature, the heat generation and the cooling power. Namely, let us compute

$$T_{av} = \frac{1}{t}\int_0^t T dt, \quad G_{av} = \frac{1}{t}\int_0^t G dt, \quad W_{av} = \frac{1}{t}\int_0^t W dt \cdot$$

The calculations presented in Figs. 7 and 8 show that there exist the corresponding stable averaged values around which the stable fluctuations occur after the transition period. Their existence depicts that there must be the relationship between them, which allow to define the stability boundary during AC regimes. The results presented in Fig. 9, which were made at f = 10 Hz (Fig. 9a) and f = 100 Hz (Fig. 9b), prove that the stability boundary of AC regimes may be defined analyzing the averaged values of removal efficiency of the Joule heating into the coolant. Accordingly, the stability condition has the following form

$$G_{av}(T_{av,q}) = W_{av}(T_{av,q}), \ \partial G_{av}(T_{av,q})/\partial T = \partial W_{av}(T_{av,q})/\partial T$$

in the zero-dimensional approximation. Here, $T_{av,q}$ is the average thermal runaway temperature (Figs. 7a and 8a).
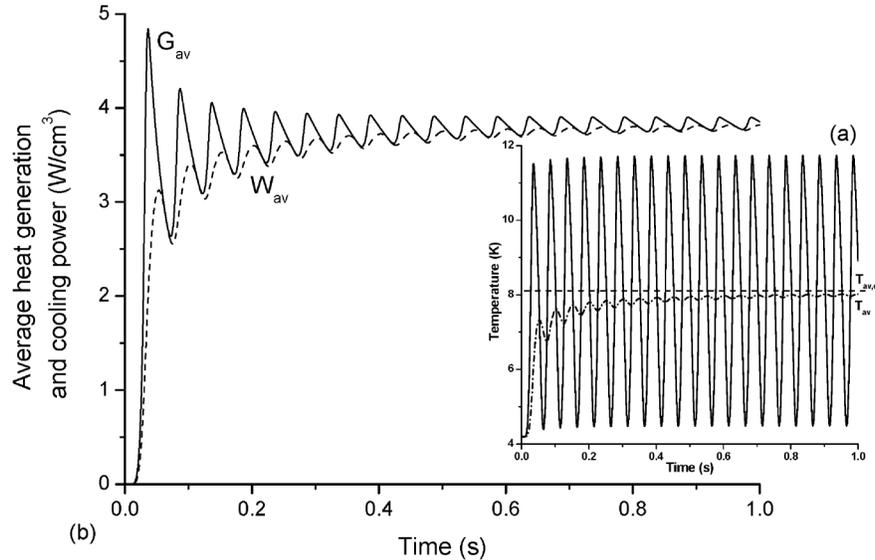

Fig. 7. Stable evolution of temperature and average values of temperature (a), heat generation and cooling power (b) at f = 10 Hz

Fig. 10 shows the dependence of the maximum possible changes of temperature, T_{max} (Fig. 10a); heat generation, G_{max}, (Fig. 10b) and current, I_{max}, (Fig. 10c) on the frequency in a superconductor during stable AC overloaded regimes. The corresponding thermal runaway values of the temperature T_q, current I_q and average thermal runaway temperature $T_{av,q}$ are also depicted. The results presented demonstrate the following features. First, allowable fluctuations of temperature are very small at low frequency because the current instability may happen in the first output mode when its duration is relatively large. In this case, the output time of current is larger than the time of the instability development. Thereby, the values of T_{max} and I_{max} are close to the corresponding thermal runaway temperature T_q and current I_q. Second, the stable range of the temperature fluctuation and limiting overloaded currents increase with increasing frequency because the duration of the first stage decreases. Third, at high frequencies, the stable range of the peak temperature and average temperature fluctuation decrease with increasing frequency. The reasons of these features are as follows. The temperature of superconductor is proportional to the heat dissipation. It will have maximum (figure 10b) as, first of all, the maximum value of the peak electric field will be also non-monotonous function of frequency. Indeed, the induced electric field will increase with increasing current frequency at small values of *f*. At the same time, it will be decreasing function of the frequency at their high values because the higher frequency, the smaller the time during which the maximum value of the peak electric field is reached. Fig. 11 depicts the corresponding dependences of the dynamics of induced electric field and temperature on the frequency.
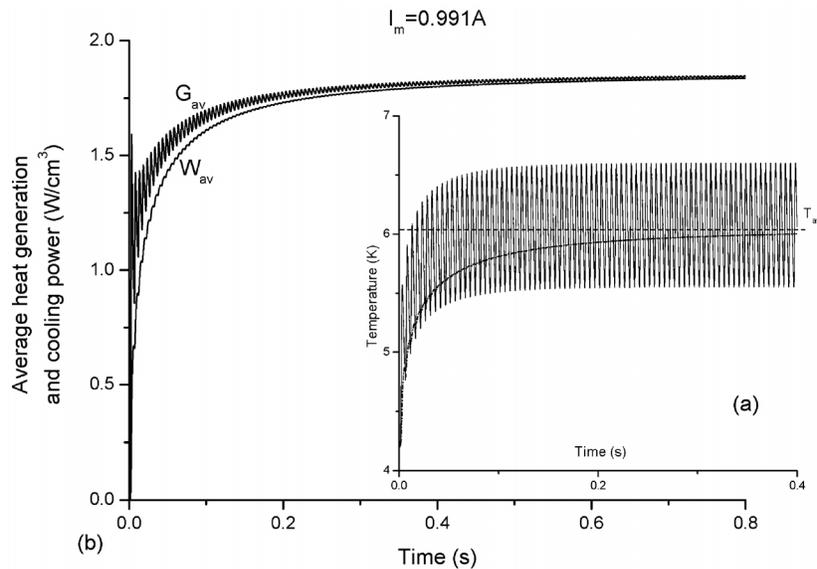

Fig. 8. Stable evolution of temperature and average values of temperature (*a*), heat generation and cooling power (*b*) at *f* = 100 Hz
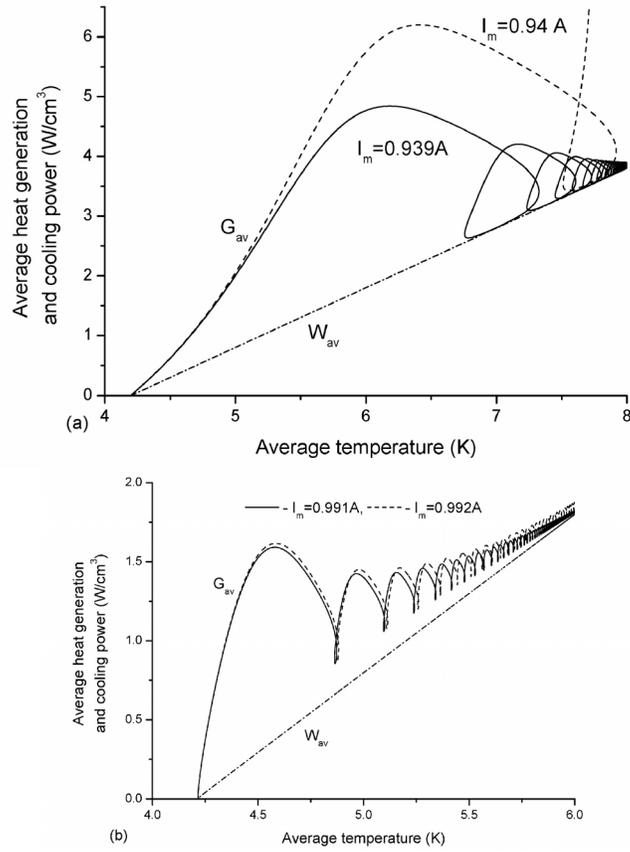
Fig. 9. Average values of heat generation and cooling power as a function of average temperature near AC stability boundary:
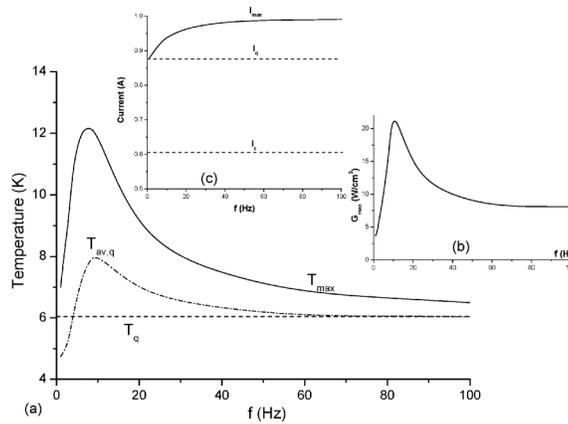*(a) - f = 10 Hz, (b) - f = 100 Hz.*

Fig. 10. Influence of the frequency on the limiting stable values of the temperature peak, average thermal runaway temperature (*a*), heat generation (*b*) and peak values of current (*c*)
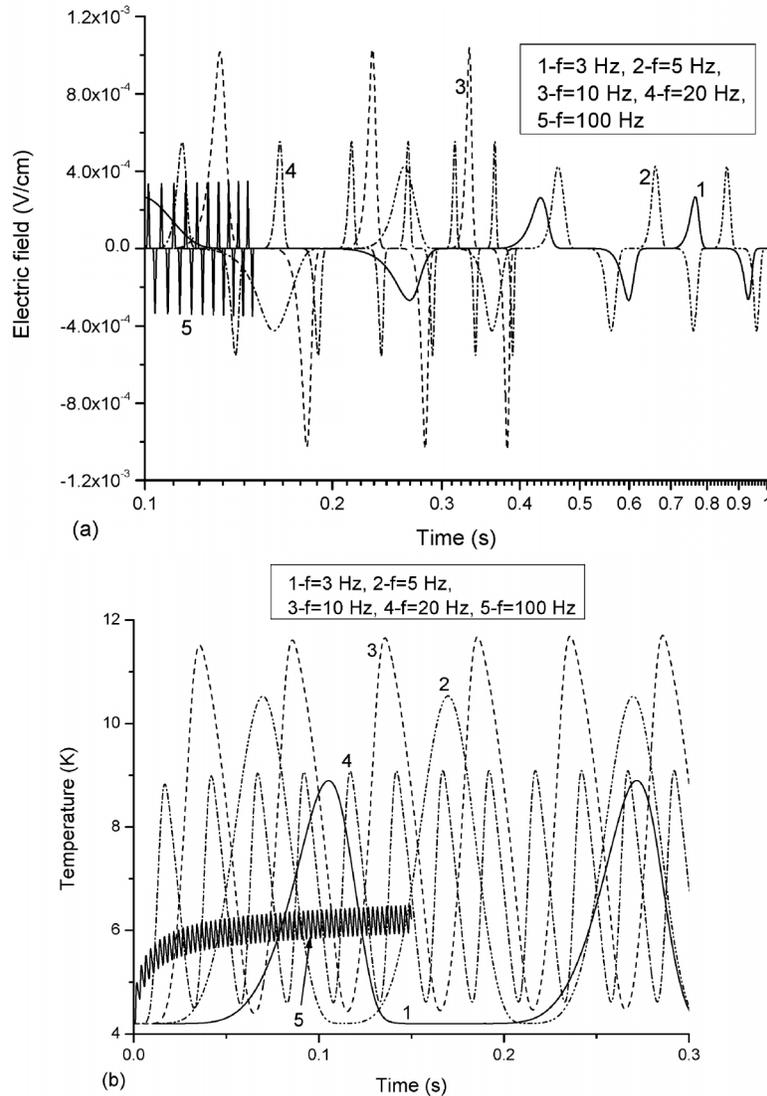
Fig. 11. Frequency effect on the evolution of electric field (a) and temperature (b) before current instability:
1-I_m=0.895 A, 2-I_m=0.910 A, 3-I_m=0.939 A, 4-I_m=0.967 A, 5-I_m=0.993 A.

Along with this, the values of I_{max} monotonously increase to the saturated value even when the temperature of the fluctuations decreases and tends to its limit that equals T_q at high frequency. This existence of the saturated value of I_{max} is a result of the formation peculiarities of all stages discussed above.

4. AC INSTABILITY OF SUPERCONDUCTING WIRES AND TAPES

Let us investigate the stability mechanisms of AC overloaded regimes in the high-T_c superconducting tape -a<x<a, -b<y<b, -∞<z<∞, b>>a). Let us assume that

- The silver-sheathed $Bi_2Sr_2CaCu_2O_8$ superconducting tape with the cross-sectional area $S=4ab$ has filaments with small transverse sizes, which are evenly distributed over a cross-sectional of a tape with the volume fraction coefficient η;
- The external magnetic field is parallel to its surface and penetrates over the cross-sectional area of tape;
- The applied sinusoidal current is charged in the z-direction and its self-field is greatly less than the external magnetic field.

The results of the simulation discussed below were made at T_0=4.2 K assuming that the background magnetic field is equal to B=10 T and the heat removal conditions on the surfaces of the tape are close to the conduction-cooling condition (h=10^{-3} W/(cm^{2}K)). The values of the critical current density J_{c0}, peak current I_m and sheath resistance ρ_n were varied.

Under these assumptions, the following zero-dimensional set of equations

$$C(T)dT / dt = -h(T - T_0) / a + E(t)J(t), \quad T(0) = T_0 \tag{10}$$

$$E(t) = E_c \left[J_s(t) / J_c(T,B) \right]^n = J_n(t)\rho_n(T,B), \quad E(0) = 0 \tag{11}$$

$$J(t) = \eta J_s(t) + (1-\eta)J_n(t), \quad J(t) = I_m \sin(2\pi ft) / S \tag{12}$$

should be used to describe the spatially uniform distribution of the temperature and electric field in the framework of the continuous medium model. Here, the heat capacities of the superconductor C_s and the sheath C_n are taken into account to calculate the heat capacity of the tape as follows

$$C(T)=\eta C_s(T)+(1-\eta)C_n(T)$$

The heat capacity of silver C_n was calculated in accordance with [35]. The characteristic values of the residual resistivity ratio RRR=ρ_n(273 K)/ρ_n(4.2 K) were varied assuming that ρ_n(273 K)=1.48×10^{-6} Ω·cm according to [35]. The sheath resistivity ρ_n as a function of temperature and magnetic field was approached by the relations proposed in [35,36]. The dependence of the critical current on the temperature is approximated by (4). The following parameters a = 0.019 cm, b = 0.245 cm, η = 0.2, n = 10, E_c = 10^{-6} V/cm, T_{cB} = 26.12 K were set.

Figs. 12 and 13 show the existence of the stability boundary of AC overloaded regimes, which takes place at f = 10 Hz during current charging into the superconducting tapes with different critical currents and resistivity of sheath. The critical current of the tape was equal to 56.6 A for the calculations presented in Fig. 12 and 566 A for the results illustrated in Fig. 13. The calculations show that the thermal runaway values of electric field, current and temperature equal E_q = 3.57×10^{-6} V/cm, I_q = 74 A, T_q = 6.91 K and E_q = 2.9×10^{-6} V/cm, I_q = 573 A, T_q = 5.9 K, respectively to the above-mentioned critical currents for the superconducting tapes with high resistive sheath (RRR=10).
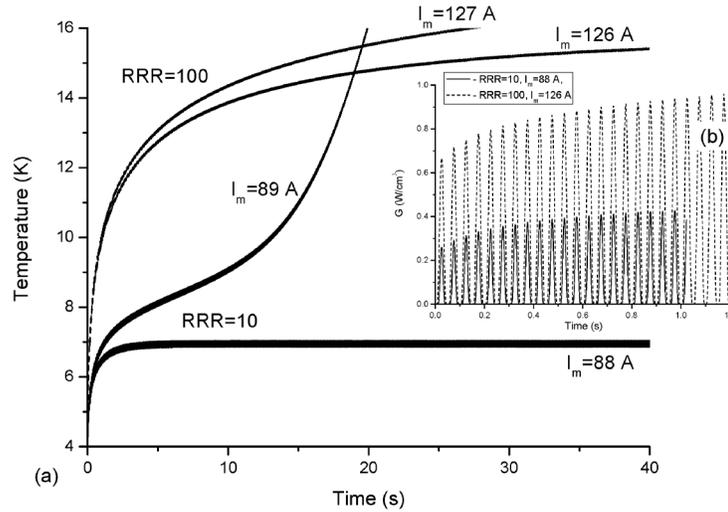
Fig. 12. Stable and unstable evolution of temperature (*a*) and heat generation power (*b*) near the stability boundary at $J_{c0}=1.52\times10^4$ A/cm^2.
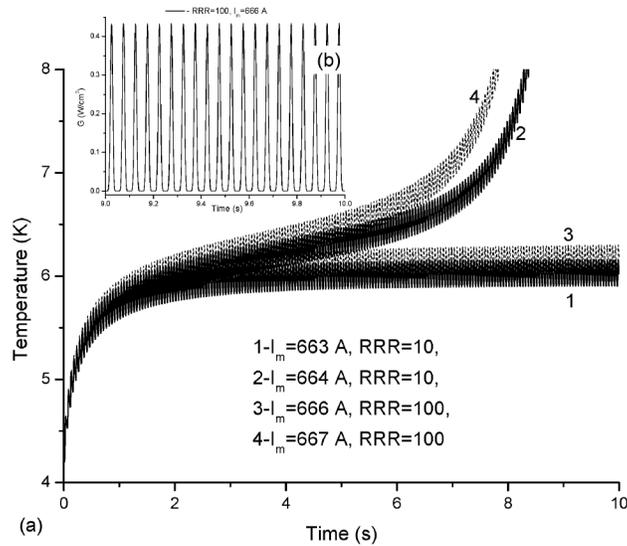

Fig. 13. Stable and unstable evolution of temperature (*a*) and heat generation power (*b*) near the stability boundary at $J_{c0}=1.52\times10^5$ A/cm^2

It is seen that the typical transient stable and unstable modes will be observed in superconducting tape near the AC stability boundary. Thereby, the limiting peak current exists and it defines the stability boundary of the AC overloaded operational regimes, which are either maintained or lost superconducting properties. Accordingly, the stability boundary is uniquely specified by the dynamic equilibrium between the averaged values of G_{av} and W_{av} at average thermal runaway temperature $T_{av,q}$ (Fig. 14). Besides, the current of AC instability, induced electric field and temperature are also higher than the corresponding critical values. However, the AC heat generation at RRR=10 and, thereby, the temperature

of the tape with high resistive matrix are less before instability than in the case of a superconductor without stabilizing matrix. This result is due to the low engineering value of the critical current density of the tape that is equal to ηJ_c. The simulation also shows that the lower the critical current, the higher the influence of the sheath resistivity on the operating modes before instability. In particular, the lower the resistivity, the higher the current in the sheath (Fig. 15). As a result, stable AC losses and the temperature rise at RRR=100 will be essentially exceed the ones in the case RRR=10. These regularities are due to the damping effect of the sheath. Along with this, the sheath influences on the evolution of its stable AC overloaded regimes. Figs. 16 and 17 show the features of the formation stages, which take place in a superconducting tape before instability onset. Accordingly, there are four stages only at very low frequency of the charged current (Fig. 16). As calculations show, the first stage, which must exist just after I_m, is practically very short at $f < 3$ Hz for the tapes under consideration. Therefore, it is absent at f=10 Hz (Fig. 17). As a result, the current and the electric field start to decrease simultaneously in the first stage. Then the electric field and the temperature in a tape decrease at the second formation stage ($|I(t)| < I_q$) when the current changes in the range from t_{Tmax} to t_{Tmin}. Finally, in the third stage, the temperature of a tape starts to increase as $|I(t)| > I_q$. However, this stage does not lead to the instability onset because there takes place stable balance between averaged values of the heat generation and the cooling power (Fig. 14).

These peculiarities affect the AC voltage-current characteristics of superconducting tapes. Fig. 18 shows the results of the corresponding calculations that should be taken into consideration during experiments. It is clearly seen vanishingly short duration of first stage that exists between I_m and E_{max}. As a result, the limiting currents depend weakly on the frequency (Fig. 19). However, the higher the critical current or the lower the matrix resistivity, the higher the limiting peak currents.

To understand this AC behavior of superconducting tapes, let us analyze the relation between dE/dt and dI/dt in the range $E > 0$. It may be written as follows

$$\frac{dE}{dt} = \frac{\dfrac{1}{S}\dfrac{dI}{dt} + \dfrac{[G(T)-W(T)]}{C(T)}\left[\eta\left|\dfrac{dJ_c}{dT}\right|\left(\dfrac{E}{E_c}\right)^{1/n} + \dfrac{1-\eta}{\rho_m^2}\dfrac{d\rho_m}{dT}E\right]}{\dfrac{1-\eta}{\rho_m} + \dfrac{\eta J_c(T)}{nE}\left(\dfrac{E}{E_c}\right)^{1/n}}$$

according to equations (10) – (12). It shows that the duration of the first time window $\Delta t = t_{Emax} - t_m$ is the function of the frequency, the conditions of heat exchange, the volume fraction of a superconductor, temperature dependences of the critical current density, resistivity of sheath and heat capacity. Namely, the first time window will be lower when the current frequency and the heat capacity will be higher or the critical current density of a superconductor, the value d(ηJ_c)/dT, difference between the heat generation and the cooling power will be lower. As the limiting current-carrying capacity of high-T_c superconducting tapes depends on Δt, then these peculiarities lead to the fact that AC current instability conditions will depend weakly on the frequency. This conclusion is proved by Fig. 19 depicting also that the sheath of tape has effective damping properties in the AC instability phenomenon.
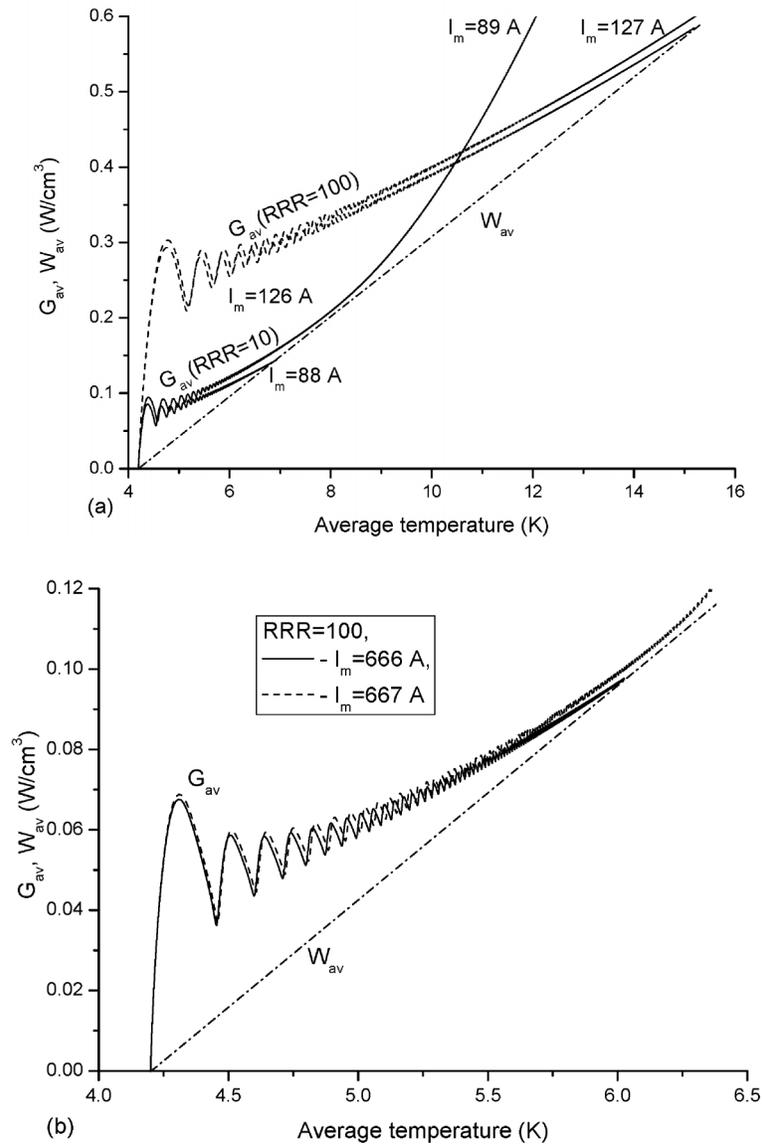
Fig. 14. Averaged values of heat generation and cooling power as a function of average temperature near AC stability boundary at different values of the critical current and matrix resistivity

(a) - $J_{c0}=1.52\times10^4$ A/cm^2, (b) - $J_{c0}=1.52\times10^5$ A/cm^2.
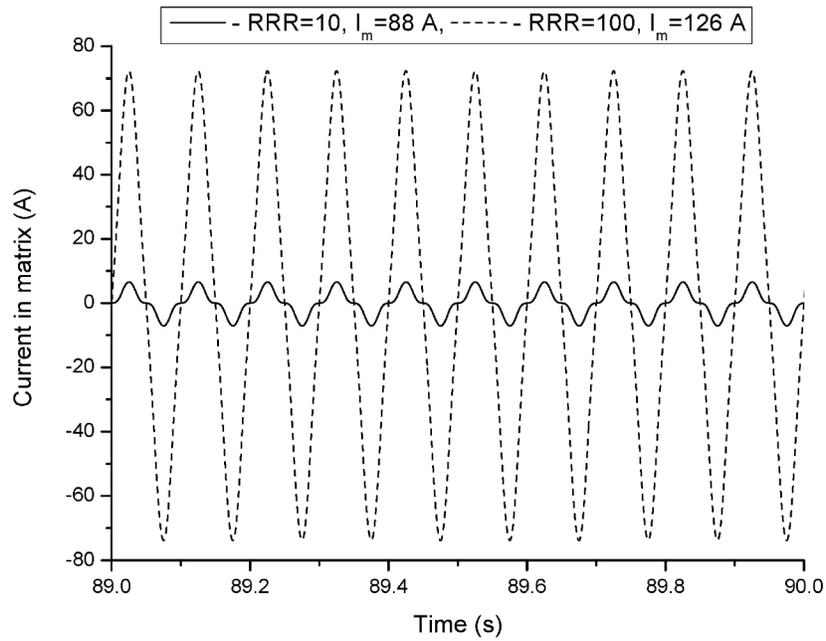
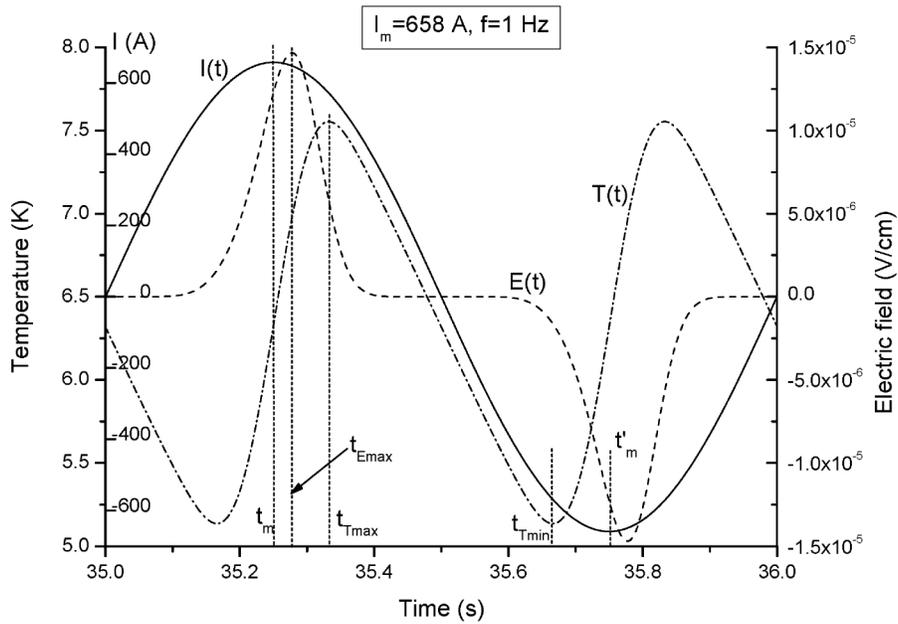**Fig. 15. Influence of RRR on the current distribution in a tape before instability**

Fig. 16. Stable formation stages of charged current, temperature and electric field at
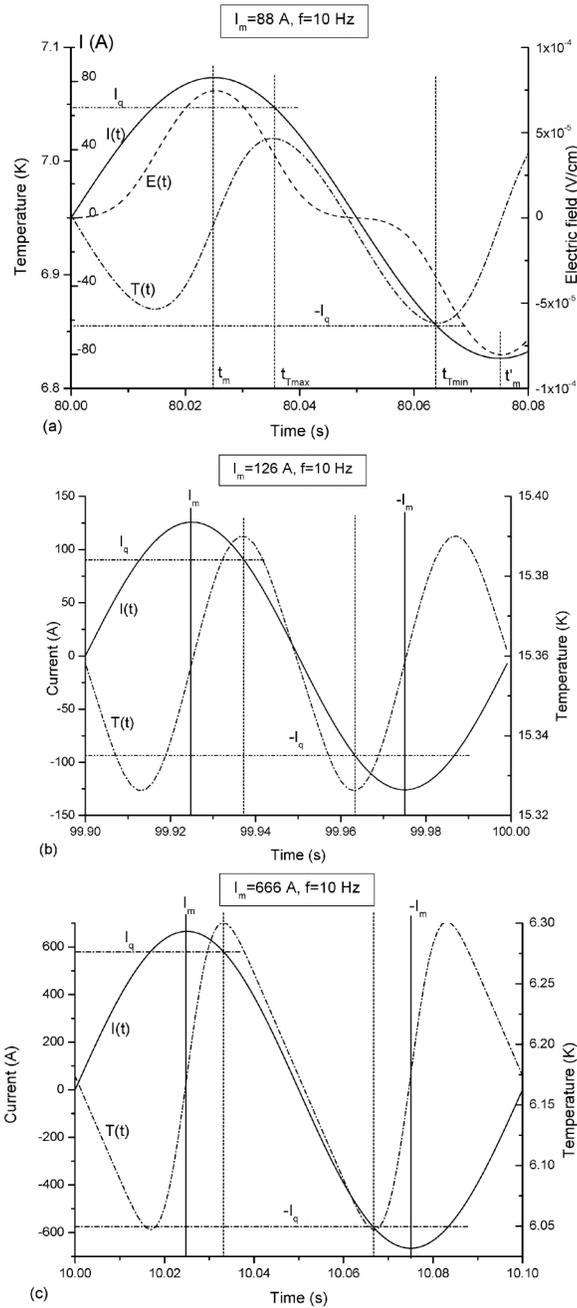f **= 1 Hz,** J_{c0}**=1.52×10⁵ A/cm² and RRR=100**

Fig. 17. Stable formation stages of operational states at *f* = 10 Hz and different values of the critical current and matrix resistivity:

(a) – charged current, temperature and electric field at $J_{c0}=1.52\times10^4$ A/cm^2 and RRR=10, (b) – charged current and temperature at $J_{c0}=1.52\times10^4$ A/cm^2 and RRR=100, (c) – charged current and temperature at $J_{c0}=1.52\times10^5$ A/cm^2 and RRR=100.
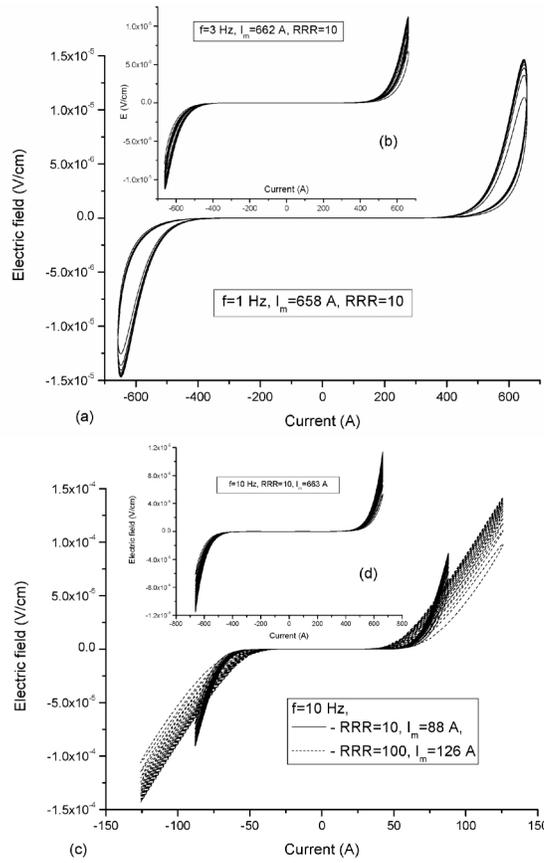
Fig. 18. Voltage-current characteristics of superconducting tape during stable AC overloaded regimes at different values of the critical currents, frequencies and RRR:
(a, b) - J_{c0}=1.52×10^5 A/cm^2 ; (c, d) - J_{c0}=1.52×10^4 A/cm^2 .
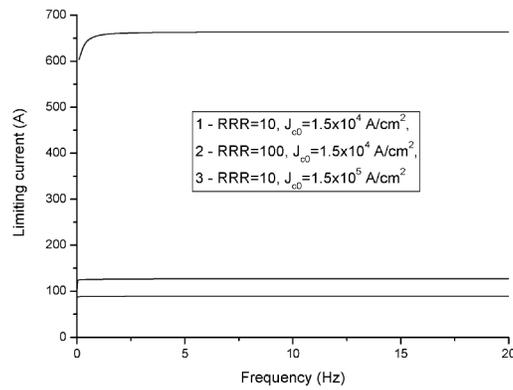

Fig. 19. Influence of the current frequency on AC limiting current-carrying capacity of superconducting tape.

5. CONCLUSION

The current instability mechanisms are studied during AC overloaded regimes in high-T_c superconductors and superconducting tapes. It is shown that the stable formation of AC overloaded regimes has the stages, which are defined by characteristic time windows. They exist due to the dynamic thermal equilibrium between the average values of heat generation and the average values of heat removal to a coolant despite the high stable overheating of a superconductor and the induced electric field. Therefore, the high-T_c superconductors may save the superconducting state during the AC overloaded modes or jump into an unstable state during ones. This feature defines the existence of the maximum value of the peak current of stable AC overloaded regimes at the given frequency and cooling conditions. In all cases, this value is higher not only the critical current of a superconductor but also the corresponding thermal runaway current defining the current stability boundary in the DC regimes. Besides, stable peak values of the electric field and temperature are also higher than the related thermal runaway values.

Thus, the presented results prove that the application of the AC overloaded regimes for many superconducting electro-power devices would be very successful. Besides, they also should be taken into consideration when the range of stable losses in high-T_c superconductors is defined. In these AC overloaded regimes, the stable temperature rise of a superconductor is very high and the standard AC losses theory, which is based on the isothermal approximation, cannot be used.

ACKNOWLEDGMENTS

COMPETING INTERESTS

The authors confirm that this article content has no conflicts of interest.

REFERENCES

1. Kruchinin S, Nagao H, Aono S. Modern aspect of superconductivity: theory of superconductivity. Singapore: World Scientific Publishing; 2010.
2. Kruchinin SP. Physics of high-T_c superconductors. Review in Theoretical Physics. 2014;2:1 – 22.
3. Kruchinin SP, Zolotovsky A, Kim HT. Andreev state in hybrid superconducting nanowires. Quantum Matter. 2014;3:1 – 4.
4. Wilson MN. Superconducting magnets. Oxford: Clarendon Press; 1983.
5. Gurevich AV, Mints RG, Rakhmanov AL. The physics of composite superconductors. NY: Beggel House; 1997.
6. Zeldov E, Amer NM, Koren G, et al. Flux creep characteristics in high-temperature superconductors. Appl Phys Lett. 1990;56:680 – 2.
7. Šouc J, Gömöry F, Janíková E. *I-V* curve of Bi-2223/Ag tapes in overload conditions determined from AC transport data. Physica C – Supercond Appl. 2004;401:75-9.
8. Ishiyama A, Yanai M, Morisaki T, *et al*. Transient thermal characteristics of cryocooler-cooled HTS coil for SMES. IEEE Trans Appl Supercond. 2005;15:1879-1882.

9.   Lue JW, Gouge MJ, Duckworth RC. Over-current testing of HTS tapes. IEEE Trans Appl Supercond. 2005;15:1835-8.
10.   Polak M, Hlasnik I, Krempasky L. Voltage-current characteristics of Nb-Ti and Nb_3Sn superconductors in flux creep region. Cryogenics. 1973;13:702–711.
11.   Kalsi SS, Aized D, Connor B, et al. HTS SMES magnet design and test results. IEEE Trans on Appl Supercon. 1997;7:971- 5.
12.   Kumakura H, Kitaguchi H, Togano K, et al. Performance test of Bi-2212 pancake coils fabricated by a lamination method. Cryogenics. 1998;38:163-7.
13.   Kumakura H, Kitaguchi H, Togano K, et al. Performance test of Bi-2223 pancake magnet. Cryogenics. 1998;38:639 - 643.
14.   Wetzko M, Zahn M, Reiss H. Current sharing and stability in a Bi-2223/Ag high temperature superconductor. Cryogenics. 1995;35:375-386.
15.   Kiss T, Vysotsky VS, Yuge H, et al. Heat propagation and stability in a small high-T_c superconductor coil. Physica C-Supercond Appl. 1998;310:372-6.
16.   Lehtonen J, Mikkonen R, Paasi J. Stability considerations of a high-temperature superconductor tape at different operating temperatures. Physica C-Supercond Appl 1998;310:340-4.
17.   Lehtonen J, Mikkonen R, Paasi J. A numerical model for stability considerations in HTS magnets. Supercond Sci Technol. 2000;13:251-8.
18.   Rakhmanov AL, Vysotsky VS, Ilyin YA, et al. Universal scaling low for quench development in HTSC devices. Cryogenics. 2000;40:19 - 27.
19.   Romanovskii VR, Watanabe K, In: Superconducting Magnets and Superconductivity, Editors H. Tovar and J. Fortier, Nova Science Publishers Inc., New York, USA. 2009; 293-399.
20.   Romanovskii VR, In: Superconductivity: Theory, Materials and Applications, Editor V.R. Romanovskii, Nova Science Publishers Inc., New York, USA (2012) 111-198.
21.   Majoros M, Glowacki BA, Campbell AM. Stability of Bi-2223/Ag multifilamentary tapes with oxide barriers – a numerical simulation. Physica C– Supercond Appl. 2002;372-376:919 – 922.
22.   Rettelbach T, Schmitz GJ. 3D simulation of temperature, electric field and current density evolution in superconducting components. Supercond Sci Technol. 2003;16:645 − 653.
23.   Newson MS, Ryan DT, Wilson MN, et al. Progress in the design and operation of high-T_c coils using dip-coat BSCCO-2212/Ag Tape. IEEE Trans on Appl Supercon. 2002;12:725-8.
24.   Watanabe K, Awaji S, Motokawa M. Cryogenfree superconducting magnets. Physica B. 2003;329-333:1487 − 8.
25.   Bellis RH, Iwasa Y. Quench propagation in high T_c superconductors. Cryogenics. 1994;34:129-144.
26.   Tanaka H, Furuse M, Arai K, et al. Thermal runaway and resistive properties of a Bi2223 pancake coil subjected to overcurrent. IEEE Trans on Appl Supercon. 2005;15:2094 – 7.
27.   Nishijima G, Awaji S, Hanai S, et al. 18.1 T Cryocooled Superconducting Magnet with a Bi2223 High-T_c Insert. Fusion Engin Design. 2006;81:2425-2432.
28.   Weijers HW, Trociewitz UP, Markiewicz WD, *et al*. High field magnets with HTS conductors. IEEE Trans Appl Supercond. 2009;20:576-582.
29.   Friend CM, Miao H, Huang Y, *et al*. The development of high field magnets utilizing Bi-2212 wind & react insert coils. IEEE Trans Appl Supercond. 2009;20:583-6.
30.   Junod A, Wang KO, Tsukamoto T, *et al*. Specific heat up to 14 tesla and magnetization of a $Bi_2Sr_2CaCu_2O_8$ single crystal. Physica C-Supercond Appl. 1994;229: 209-230.

31. Herrmann PF, Albrecht C, Bock J, *et al*. European Project for the development of High T_c Current Leads. IEEE Trans Appl Supercon. 1993;3:876-880.
32. Watanabe K, Romanovskii VR, TakahashiK, *et al*. Current-carrying properties in a low resistive state for Ag-sheathed $Bi_2Sr_2CaCu_2O_8$ tape. Supercond Sci Technol. 2004;17:S533-7.
33. Romanovskii V, Lavrov N, Ozhogina V. Stable and unstable thermo-current states of high temperature superconductors. J Phys: Conf Ser. 2008;97:012017.
34. Keilin VE, Romanovskii VR, Superconducting state stability in current charging into composite. Cryogenics. 1993;33:986 -994.
35. Dresner L. Stability and protection of Ag/BSCCO magnets operated in the 20-40K range. Cryogenics. 1993;33:900-9.
36. Lim H, Iwasa Y. Two-dimensional normal zone propagation in BSCCO-2223 pancake coils. Cryogenics. 1997;37:789 -799.

APPENDIX

Let us investigate in one-dimensional approximation the AC stability problem of current charged into superconducting slab considered in Section 3. Suppose that the applied current is charged in the *y*-direction and it has a serrated time mode (triangular-wave) with the constant charging rate $\pm dI/dt$ and the peak current I_m. Accordingly, let us define distribution of the temperature, electric field and current density, which are independent of *z* and *y* coordinates, using the one-dimensional model described by equations (1) - (7). In the serrated mode under consideration, the current as a function of time is simulated as

$$I(t) = \begin{cases} \dfrac{dI}{dt}t, & t \le t_1 \\ \pm I_m \mp \dfrac{dI}{dt}(t - t_{2k-1}), & t_{2k-1} < t < t_{2k+1}, \quad t_k = \dfrac{I_m}{dI/dt}k, \quad k = 1,2,3,... \end{cases}.$$

Fig. 20 depicts the characteristic stages of the overloaded state evolution during serrated time mode. The results presented were obtained numerically under parameters $a = 10^{-3}$cm, $b = 10^{-2}$ cm, $dI/dt = 10$ A/s, $I_m = 0.93$ A, $T_0 = 4.2$ K, $E_c = 10^{-6}$ V/cm, $J_{c0} = 1.52 \times 10^4$ A/cm^2, $T_{cB} = 26.12$ K, $n = 10$. The specific heat capacity and thermal conductivity of the superconductor were defined as it was made above. The corresponding values of the critical electric field, thermal runaway electric field and thermal runaway temperature are also shown in Fig. 20.

The results presented show the existence of the characteristic times t_m, t_{Emax}, t_{Tmax} and t_{Tmin}. They define the characteristic formation time windows of the AC overloaded states as it was formulated above. Namely, $t = t_m$ is the time when charged current is equal to the peak value of the applied current I_m; t_{Emax} is the time when the electric field has the maximum; t_{Tmax} is the time when temperature of the superconductor has the maximum at which the heat generation becomes equal to the heat removal; t_{Tmin} is the time after which the heat generation exceeds the heat removal and the temperature of superconductor stars to increase. Thus, the used one-dimensional approximation proves the general physical conclusions formulated above that were made without a large volume of calculations using simplified zero-dimensional approximation.
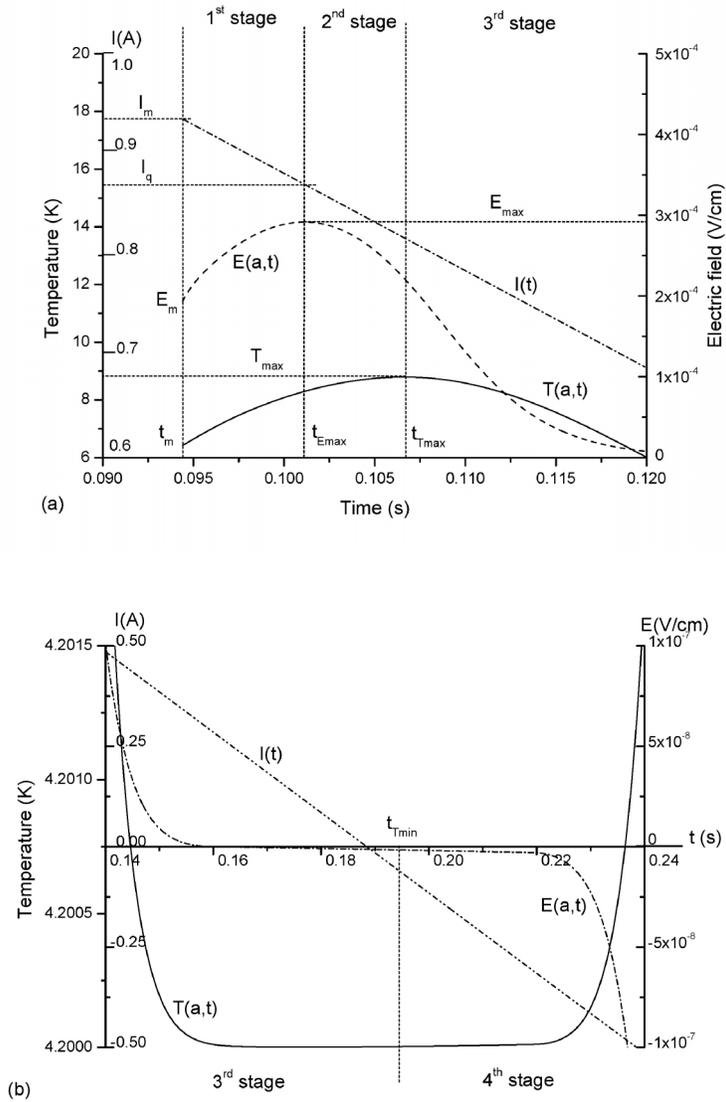
Fig. 20. One-dimensional simulation of thermo-electrodynamics states of superconductor in the overloaded serrated time mode